Atmospheric Pollution Research 7 (2016) 743–753

Contents lists available at ScienceDirect

Atmospheric Pollution Research

journal homepage: http://www.journals.elsevier.com/locate/apr

Original article

# Calibration of the 936 nm water-vapor channel for the China aerosol remote sensing NETwork (CARSNET) and the effect of the retrieval water-vapor on aerosol optical property over Beijing, China

Huizheng Che [a, b, *], Ke Gui [b, a], Quanliang Chen [b, **], Yu Zheng [a, c], Jie Yu [a, b], Tianze Sun [a], Xiaoye Zhang [a], Guangyu Shi [d]

[a] State Key Laboratory of Severe Weather (LASW), Institute of Atmospheric Composition, Chinese Academy of Meteorological Sciences, Beijing, 100081, China
[b] College of Atmospheric Science, Chengdu University of Information Technology, Plateau Atmospheric and Environment Laboratory of Sichuan Province, Chengdu, 610225, China
[c] Key Laboratory for Aerosol-Cloud-Precipitation of China Meteorological Administration, Nanjing University of Information Science and Technology, Nanjing, 210044, China
[d] State Key Laboratory of Numerical Modeling for Atmospheric Sciences and Geophysical Fluid Dynamics (LASG), Institute of Atmospheric Physics, Chinese Academy of Sciences, Beijing, 100029, China

ARTICLE INFO

*Article history:*
Received 14 November 2015
Received in revised form
15 March 2016
Accepted 6 April 2016
Available online 25 April 2016

*Keywords:*
CE-318 sunphotometer
Calibration
Modified langley method
CARSNET
Columnar water-vapor

ABSTRACT

Based on measurements of the 936 nm water-vapor channel and the 870 nm, and 1020 nm atmospheric window band for the CE-318 sunphotometer of CARSNET, clear-sky direct solar radiation observational data and relative optical air masses of between 2 and 5, and considering sensitivity parameters such as pressure, altitude, wavelength, and $AOD_{936nm}$, which may affect the calibration result, a method to calibrate the 936 nm water-vapor channel using a modified Langley method is presented. The daily average columnar water-vapor (CWV) over urban Beijing was retrieved using three methods (Methods A, B and C), and compared with the AERONET water-vapor product. Finally, the seasonal relationships of CWV with $AOD_{500nm}$ and $\alpha_{440-870}$ were analyzed. The calibration results showed the calibration value to differ from the original value by about 4%. The CWV retrieval result showed that AERONET and the three methods of retrieval for CWV were highly correlated. The monthly average variation trends of $AOD_{500nm}$ and CWV were similar, with the maximum occurring in July, and the minimum in December. The seasonal average variation trends of $AOD_{500nm}$ and CWV were also similar, but could be placed in the following order: summer > autumn > spring > winter. The seasonal variation of $\alpha_{440-870}$ versus $AOD_{500nm}$, $\alpha_{440-870}$ versus CWV, and $AOD_{500nm}$ versus CWV, showed increasing $AOD_{500nm}$ with increasing CWV, which reflected the hygroscopicity of aerosol fine particle growth characteristics. Summer was mainly characterized by fine particles; while spring, autumn and winter were a mix of coarse and fine particles, showing typical urban aerosol properties.



## 1. Introduction

Water vapor is an important component of the atmosphere. Not only is it a key greenhouse gas, but it also plays an important role in the growth of aerosol. In addition, water vapor affects the energy budget of the Earth's atmosphere, which drives and maintains its motions. Many techniques have been developed for measuring water vapor content. Currently, columnar water-vapor (CWV) data are acquired by satellite remote sensing instruments, radiosondes, sun photometers, microwave radiometers, lidars, and global positioning system receivers; and in recent years, a large number of papers have been published on the topic of CWV retrieval by ground-based sun photometers (Plana-Fattori et al., 1998; Schmid et al., 2001; Zhang et al., 2006, 2009; Campanelli et al., 2010; Campmany et al., 2010; Zhou and Liu, 2011; Campanelli et al., 2014).

* Corresponding author. State Key Laboratory of Severe Weather (LASW), Institute of Atmospheric Composition, Chinese Academy of Meteorological Sciences, Beijing, 100081, China. Tel.: +86 10 5899 3116; fax: +86 10 6217 6414.
** Corresponding author.
*E-mail addresses:* chehz@camscma.cn (H. Che), chenql@cuit.edu.cn (Q. Chen).
Peer review under responsibility of Turkish National Committee for Air Pollution Research and Control.

http://dx.doi.org/10.1016/j.apr.2016.04.003

Calibration is very crucial for maintaining and establishing accurate databases derived from ground-based monitoring networks (WMO, 2005). Many factors, such as instrument precision, the algorithms used, and calibration procedure, can affect the instrument calibration (Holben et al., 1998). The Cimel CE-318 instrument is a motor-tracked sunphotometer, which points automatically to the Sun (Cimel, 2001). This instrument is a standard sun/sky photometer from the Aerosol Robotic NETwork (AERONET) (Holben et al., 1998). The China Aerosol Remote Sensing Network (CARSNET) is a ground-based aerosol monitoring network that uses the same CE-318 sun photometers as AERONET (Che et al., 2009). A large number of studies have shown that uncertainty in the measurements, calibration and calculations may bring about errors. The total influence of both sources of systematic uncertainty can propagate a total systematic uncertainty of approximately ±10% in AERONET water vapor product (Smirnov et al., 2004; Alexandrov et al., 2009). Pérez-Ramírez et al. (2014) stated that CWV obtained by AERONET is lower than those obtained by MWR, GPS and radiosondes by~6.0–9.0%, ~6.0–8.0% and ~5%, respectively.

While the total standard uncertainty of CWV obtained by the optical method is approximately 10% (Schmid et al., 1996; Ingold et al., 2000), the error caused by the sunphotometer measurement itself is only approximately 0.5% (Galkin et al., 2010). The accuracy of the CWV estimate depends closely on the quality of the sunphotometer's calibration within the channel centered at 936 nm (Campanelli et al., 2010). Therefore, to obtain accurate CWV, an accurate calibration process for the water vapor band at 936 nm must be established. An intercomparison calibration method of field instrumentation was established in 2008 (Che et al., 2009). A sphere calibration method and protocol has been established for CARSNET (Tao et al., 2014). However, a CARSNET calibration process for the water vapor band at 936 nm is lacking, which hinders the retrieval of CWV using direct sun radiance observational data. The aim of the present study, therefore, was to establish a complete calibration process for the water vapor band at 936 nm for CARSNET, which will help improve the accuracy of CWV retrieval.

## 2. Instruments and measurement data

The CE-318 makes direct spectral solar radiation measurements within a 1.2° full field of view at about 15 min intervals in eight normal bands (340, 380, 440, 500, 675, 870, 1020 and 1640 nm) and one water vapor band at 940 nm. The bandwidth of each channel is 10 nm. Measurements at 340, 380, 440, 500, 675, 870, 1020 and 1640 nm are used to calculate aerosol optical depth (AOD), and measurements at 940 nm are used to retrieve CWV.

The sunphotometer used at the Chinese Academy of Meteorological Science [CAMS; CARSNET & AERONET no.543; (39.933°N, 116.317°E); 106 m above sea level] was calibrated in 2014 at Izana Observatory, Spain, following the AERONET calibration protocol method developed in 2004 (Goloub et al., 2007).

During the calibration process for the water vapor band at 936 nm, five clear days of direct solar radiation observational data with relative optical air masses of between 2 and 5 were selected. The AOD data at CAMS were calculated using the ASTPWin software developed by Cimel Ltd.Co. To improve the accuracy, we chose Level 1.5 AOD [cloud-screened AOD, based on the work of Smirnov et al. (2000)]. To retrieve the CWV, the sunphotometer data at CAMS from June 2014 to May 2015 were used. The CWV results of the Beijing-CAMS site used in this study were Level 1.5 cloud-screened data from the AERONET dataset (http://aeronet.gsfc.nasa.gov/). The observation period is from June 2014 to May 2015.

## 3. Methodology

### 3.1. Calibration

The extraterrestrial solar radiation is attenuated by particles and molecules in the atmosphere through absorption and scattering. Sun photometry deals with the attenuation of radiation through the atmosphere and uses the Beer-Bouger-Lambert attenuated law. Particularly, in the near-infrared spectrum, around 940 nm, there are many water vapor absorption bands. In this study, the retrieval of the CWV based on measurements taken at 936 nm (water absorption peak) and 1020 nm (no water absorption) according to the 2001 spectral database (Rothman et al., 2003). So, the direct solar radiation measured in the 936 nm water vapor absorption band does not comply with the Lambert–Beer law, the Langley calibration method cannot be used for this channel. This, a modified Langley method was used instead. In general, the dependence of transmission $T_w$ on the water column abundance can be written as (Bruegge et al., 1992; Halthore et al., 1992; Schmid et al., 1996; Smirnov et al., 2004; Bokoye et al., 2007; Livingston et al., 2007)

$$T_w = \exp\left(-aw^b\right) \quad (1)$$

where $T_w$ is the water vapor partial atmospheric transmittance at 936 nm; $w(=m \times \mathrm{CWV})$ is the atmospheric path inclined water vapor content, m is relative optical air masses; The “constants” a and b are two coefficients that depend on the central wavelength position, width and shape of the photometer filter function, as well as the atmospheric pressure-temperature lapse rate and the vertical distribution of water vapor (Halthore et al., 1997; Alexandrov et al., 2009). For the AERONET V1 procedure (Holben et al., 1998), the coefficients a and b are maintained fixed and identical for all instruments based on low spectral resolution atmospheric transmittance (LOWTRAN) simulations (Kneizys et al., 1988). For the AERONET V2 procedure (Smirnov et al., 2004), coefficients a and b are computed by the HITRAN 2000 spectral database together with the line-by-line radiative transfer model (LBLRTM) radiative transfer code, whose output is convolved with recent measured filter response functions (Smirnov et al., 2004). Alexandrov et al. (2009) presented a detailed analysis of the errors in CWV retrieval due to uncertainties in water vapor absorption line parameters for the spectral database HITRAN 2000, HITRAN 2004 (Rothman et al., 2005) and ESA-WVR (Schermaul et al., 2001a, 2001b). The estimated uncertainties in multifilter rotating shadowband radiometer (MFRSR) associated with spectral databases can reach 5% (Alexandrov et al., 2009). In this study, coefficients a and b are computed by moderate spectral resolution atmospheric transmittance (MODTRAN 3.7) water vapor transmittance simulations (Halthore et al., 1997), the absorption line data used are obtained from the version of HITRAN 2001 molecular database. In the 936 nm water vapor absorption band, the response $V$ of the central wavelength of the sunphotometer to solar direct irradiance $E$ is given by (Reagan et al., 1992; Michalsky et al., 1995; Schmid et al., 2001).

$$V = V_0 R^{-2} \exp[-m\tau(\lambda)]T_w \quad (2)$$

where $V$ and $V_0$ are the output voltages of the sunphotometer and atmosphere top outside, respectively (the latter can be acquired via calibration); $m = 1/[\cos\theta + 0.1500(93.885-\theta)^{-1.253}]$ is the relative optical air mass (Kasten and Young, 1989), in which $\theta$ is the solar zenith angle, which can be calculated by time, latitude and longitude; $R^{-2}$ is correction coefficient for the Sun–Earth distance, which can be calculated with Julian days $j$ through the method put

forward by Josefsson, (1986):$R^{-2}=1+0.033\times cos(2\pi j/365.25)$; and $\tau(\lambda)=\tau_r(\lambda)+\tau_a(\lambda)$ is the atmospheric total optical depth at wavelength 936 nm, in which $\tau_a(\lambda)$ and $\tau_r(\lambda)$ are the aerosol extinction optical thicknesses and molecular Rayleigh scattering at 936 nm,respectively. Rayleigh scattering is calculated using the ground-level atmospheric pressure, as follows (Hansen and Travis, 1974):

$$\tau_r(\lambda)=0.008569\lambda^{-4}\left(1+0.0113\lambda^{-2}+0.00013\lambda^{-4}\right)(P/1013.25)e^{-0.125H} \quad (3)$$

Where $P$ is the pressure at the observation position and $H$ is altitude.

The aerosol optical thickness $\tau_a(\lambda)$ at 936 nm can be extrapolated from the AODs in the 870 nm and 1020 nm non-water vapor bands, according to the well-known Ångström formula (Angstrom, 1929)

$$\tau_a(\lambda)=\beta\lambda^{-\alpha} \quad (4)$$

Where $\alpha$ is the so-called Ångström exponent and $\beta$ is the atmospheric turbidity parameter, which is closely associated with the total number of aerosol particles, particle distribution and refractive index. The parameters $\alpha$ and $\beta$ are determined by the regression of Eq. (4), where $\lambda_1=870$ nm and $\lambda_2=1020$ nm:

$$\begin{cases}\alpha=-\dfrac{ln\dfrac{\tau_a(\lambda_1)}{\tau_a(\lambda_2)}}{\ln\left(\dfrac{\lambda_1}{\lambda_2}\right)}\\ \beta=\dfrac{\tau_a(\lambda_1)}{\lambda_1^{-\alpha}}\end{cases} \quad (5)$$

According to Eqs. (4) and (5), we can calculate $\tau_a$(936 nm).

Substituting Eq. (1) into Eq. (2) and taking the natural log on both sides,

$$\ln V+m\tau=\ln\left(V_0R^{-2}\right)-am^bCWV^b \quad (6)$$

And when the atmospheric condition is stable and clear, under the rectangular coordinate system with $m^b$ as the $x$-axis and $lnV+m\tau$ as the $y$-axis, draw a straight line, and the linear intercept is $ln(V_0R^{-2})$. The calibration value $V_0$ at 936 nm can then be calculated by the intercept.

### 3.2. Parameter sensitivity test

The sensitivity parameters on 5 February, 2015 [$P=1030.5$ hPa, $H=106$ m, $\lambda=936$ nm, $\tau_a(936\text{ nm})=0.041$] were used for a sensitivity test. Fig. 1 shows the time series plots of AOD over Beijing on February 5, 2015, in which $AOD_{936nm}$ no sharp fluctuations and vary smoothly with the solar elevation angle. The test results are shown in Fig. 2, in which the horizontal axis show these sensitivity parameters may affect the calibration result, and the vertical axis shows the error $\left(\frac{V_0(Test)-V_0(Feb-5)}{V_0(original)}\right)$ that results from the parametric variation. Looking at the error in Fig. 2, it is particularly noticeable that all calibration values increase within the scope of the parametric variation apart from when the $AOD_{936nm}$ increase makes the calibration value decrease. When the center wavelength (λ) changes from 937 nm to 940 nm, the error variation is only 0.013%–0.054%. When the pressure ($P$) changes from 1000 hPa to 850 hPa, the calibration value increases with the decrease in pressure, and the error variation is 0.072%–0.432%.

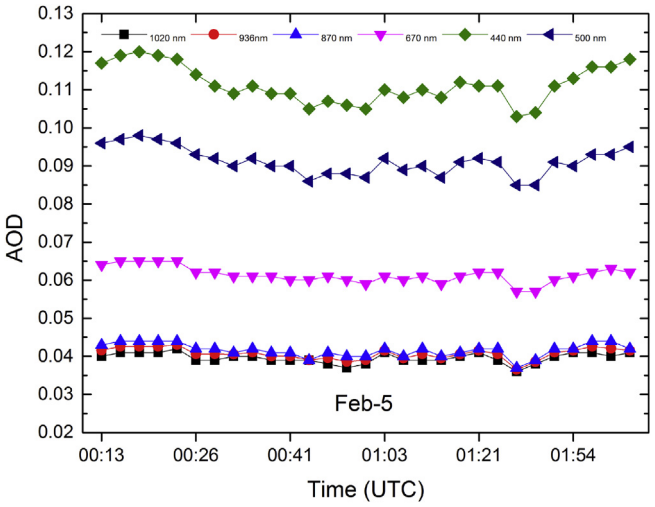


**Fig. 1.** Time series plots of AOD at 440, 500, 670, 870, 936, and 1020 nm over Beijing on February 5, 2015.

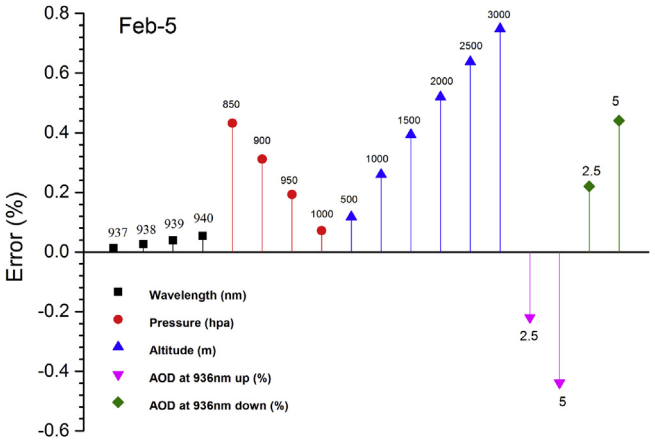


**Fig. 2.** Error results from parametric variation on 5 February.

When the altitude ($H$) changes from 500 m to 3000 m, the calibration value increases with the increase in altitude, and the error variation is 0.118%–0.749%. When the $AOD_{936nm}$ is increased by 2.5% and 5%, the error is approximately −0.220% and −0.439%, respectively. When $AOD_{936nm}$ is decreased by 2.5% and 5%, the error is approximately 0.220% and 0.441%, respectively. The test results show that different values of $AOD_{936nm}$, pressure, and altitude have a large effect on the calibration value. Moreover, when the wavelength (λ) variation is between 936 nm and 940 nm, the calibration results have little impact. Therefore, to improve the accuracy of the calibration value, these sensitivity parameters (pressure, altitude, $AOD_{936nm}$), which may affect the calibration result, must be considered.

### 3.3. CWV retrieval

1) Method A

According to Eq. (6), under the rectangular coordinate system with $m^b$ as the $x$-axis and $lnV+m\tau$ as the $y$-axis, draw a straight

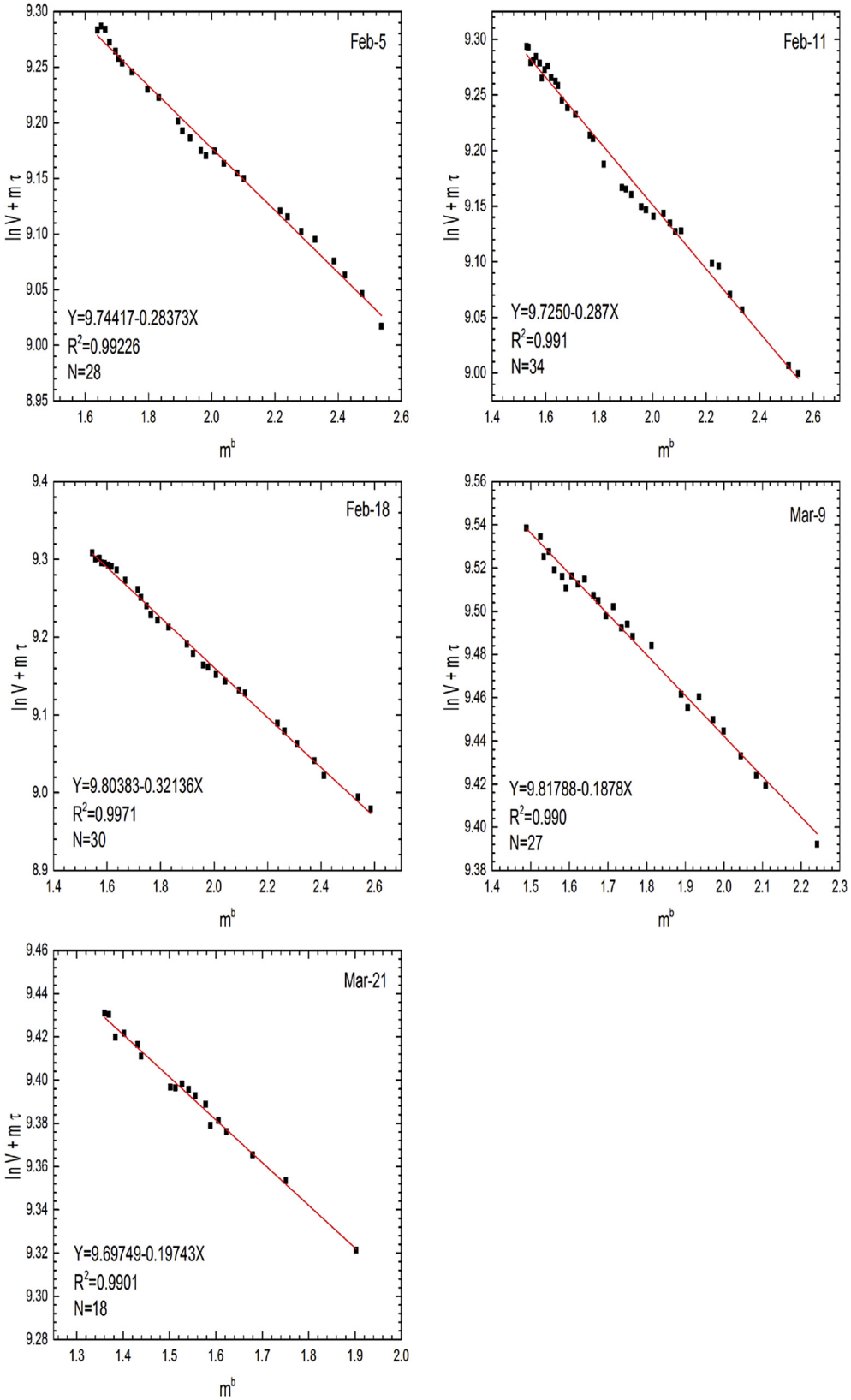


**Fig. 3.** The 936 nm water vapor channel calibration results.

**Table 1**
Comparison of calibration values and original calibration values.

| | $V_0$ | | Calibration/Original | (Calibration−Original)/Original (%) |
|---|---|---|---|---|
| | Calibration | Original | | |
| Feb-5 | 16,608 | 17,690 | 0.939 | −6.1 |
| Feb-11 | 16,327 | 17,690 | 0.923 | −7.7 |
| Feb-18 | 17,714 | 17,690 | 1.001 | 0.1 |
| Mar-9 | 18,125 | 17,690 | 1.024 | 2.5 |
| Mar-21 | 16,173 | 17,690 | 0.914 | −8.6 |
| Mean value | 16,990 | 17,690 | 0.960 | −3.96 |
| SD | 783 | – | 0.04 | – |
| RSD (%) | 4.6 | – | 4.5 | – |

**Table 2**
CWV (cm) retrieved using different methods, and their correlation coefficients.

| Date | Method A | Method B | Method C | AERONET | Correlation coefficient (r) | | |
|---|---|---|---|---|---|---|---|
| | | | | | Method A vs. AERONET | Method B vs. AERONET | Method C vs. AERONET |
| Feb-5 | 0.271 | 0.325 | 0.312 | 0.327 | | | |
| Feb-11 | 0.276 | 0.342 | 0.324 | 0.376 | | | |
| Feb-18 | 0.334 | 0.322 | 0.314 | 0.342 | 0.900 | 0.993 | 0.991 |
| Mar-9 | 0.134 | 0.119 | 0.116 | 0.125 | | | |
| Mar-21 | 0.149 | 0.222 | 0.214 | 0.221 | | | |

line, and the linear slope is $a \times CWV^b$. The CWV within a certain period of time can then be calculated by the slope.

2) Method B

Combining Eqs. (1) and (2) yields a CWV of

$$\mathrm{CWV} = \left( -\frac{\ln(\mathrm{VR}^2/\mathrm{V}_0) + \mathrm{m}\tau}{\mathrm{am}^b} \right)^{\frac{1}{b}} \tag{7}$$

With the instruments calibrated, the AERONET CWV can be computed using Eq. (7) (Reagan et al., 1992; Bruegge et al., 1992; Holben et al., 1998). Instantaneous CWV can be calculated by the slope, Eq. (7).

3) Method C

Using the ratio of the water vapor channel voltage signal ($V_{936}$) and adjacent channel voltage signal ($V_{870}$),

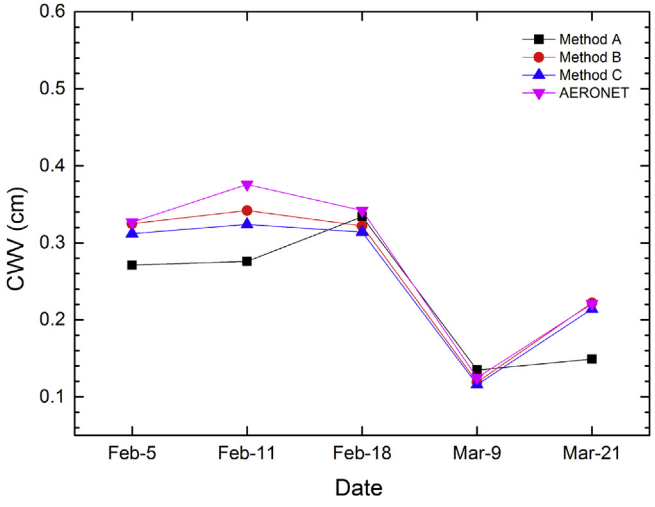


**Fig. 4.** Comparison of the CWV retrieved using Methods A, B and C, and that of AERONET.

$$\frac{\mathrm{V}_{936}}{\mathrm{V}_{870}} = \frac{\mathrm{V}^0_{936}\mathrm{e}^{-\mathrm{m}\tau_2}\mathrm{T}_w}{\mathrm{V}^0_{870}\mathrm{e}^{-\mathrm{m}\tau_1}} \tag{8}$$

Taking the natural log of this ratio yields

$$\ln\left(\frac{\mathrm{V}_{936}}{\mathrm{V}_{870}}\right) = \ln\left(\frac{\mathrm{V}^0_{936}}{\mathrm{V}^0_{870}}\right) + \mathrm{m}(\tau_1 - \tau_2) - \mathrm{a}(\mathrm{m} \times \mathrm{CWV})^{\mathrm{b}} \tag{9}$$

for the channels centered at ~870 nm and ~936 nm, respectively. $m(\tau_1-\tau_2)$ is quite small, and this term can often be neglected as a good approximation. Under the rectangular coordinate system with $m^b$ as the $x$-axis and $ln\left(\frac{V_{936}}{V_{870}}\right)$ as the $y$-axis, draw a straight line, and the linear slope is $a \times CWV^b$. The linear intercept is $\ln\left(\frac{V^0_{936}}{V^0_{870}}\right)$. The CWV within a certain period of time can then be calculated by the slope. When $V^0_{870}$ and $V^0_{936}$ have an accurate calibration value, according to Eq. (9),

$$\mathrm{CWV} = \left[ \frac{\ln\left(\frac{\mathrm{V}^0_{936}}{\mathrm{V}^0_{870}} \times \frac{\mathrm{V}_{870}}{\mathrm{V}_{936}}\right)}{\mathrm{a} \times \mathrm{m}^b} \right]^{\frac{1}{b}} \tag{10}$$

The instantaneous CWV can be calculated by the slope, Eq. (10).

### 3.4. Calibration

1) Data screening

1. Direct solar radiation observational data were selected for when the weather conditions were clear and cloudless, the atmosphere was stable, and the aerosol content was $\mathrm{AOD}_{500\mathrm{nm}} < 0.05$.
2. The data for before 10:00 a.m. were selected because, before that time, the atmosphere was relatively stable, and after, turbulent motion gradually enhanced.
3. The relative optical air mass data of between 2 and 5 were selected. The results of the sensitivity test showed that when $m < 2$, turbulent motion will keep the ground-level

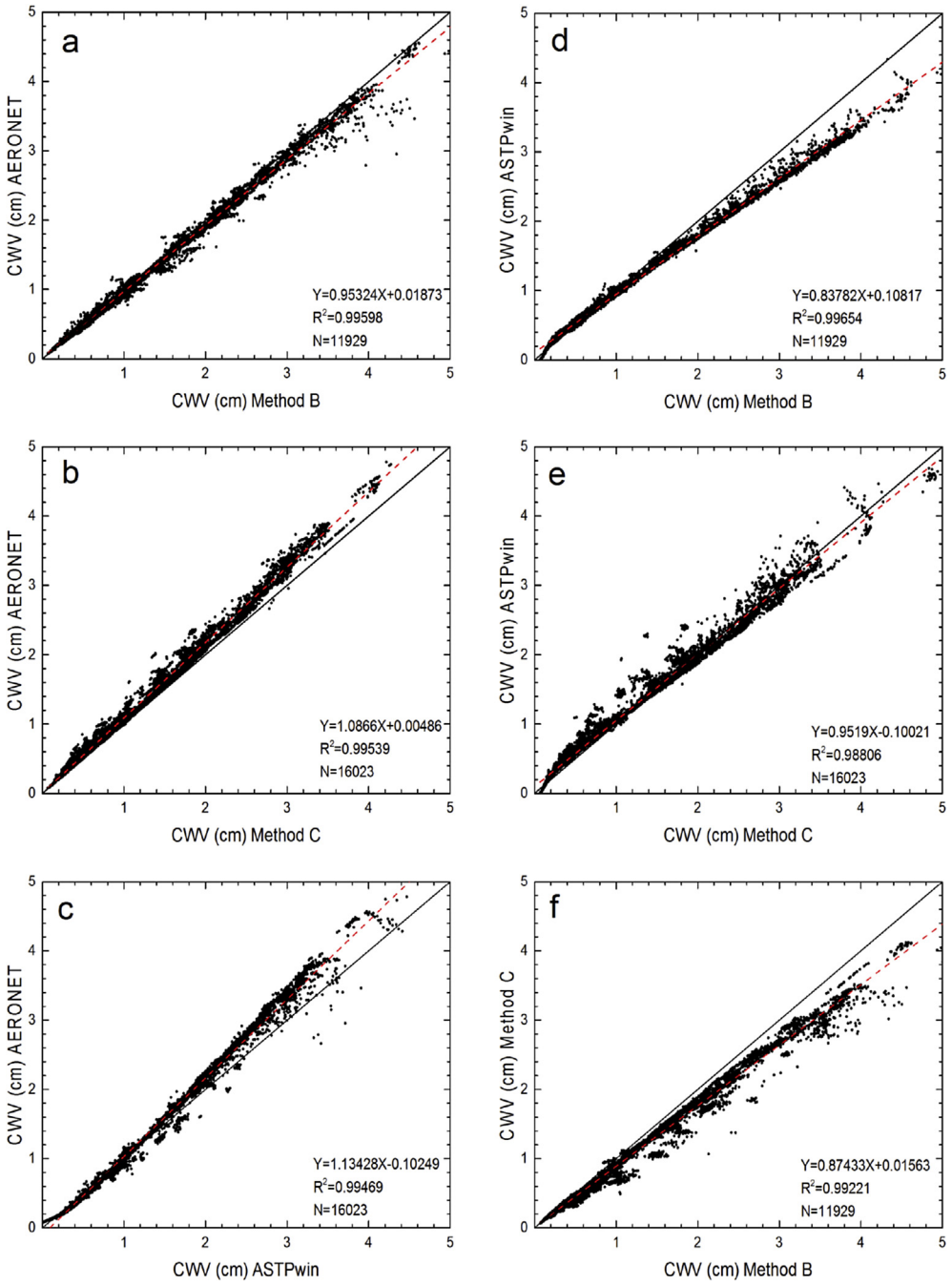


**Fig. 5.** Comparison of (a–c) Method B, Method C and ASTPWin, respectively, with AERONET, and (d–f) intercomparisons of Method B, Method C and ASTPWin.

aerosol in the air, affecting the calibration results. Meanwhile, when $m > 5$, the signal is so weak that it causes a number of error points, and these points will bring an error range of–2%–3%.

2) Data processing

The key for the calibration of the instrument in the 936 nm channel ($V_0$ (936 nm)) is to have low and stable precipitable water

**Table 3**
Comparison of CWV from various methods with the AERONET method.

| Method | n | Best fit | | | Mean | | Difference (cm) | | | | Ratio x/AERONET | |
|---|---|---|---|---|---|---|---|---|---|---|---|---|
| | | Slope | Intercept (cm) | $r^2$ | AERONET | x | Mean | Standard deviation | rms | % rms | Mean | Standard deviation |
| AERONET | | | | | | | | | | | | |
| B | 11,929 | 0.95 | 0.02 | 0.996 | 0.97 | 1.00 | 0.03 | 0.07 | 0.08 | 5.9 | 1.01 | 0.06 |
| C | 16,023 | 1.09 | 0.01 | 0.995 | 1.00 | 0.92 | −0.08 | 0.10 | 0.13 | 9.4 | 0.92 | 0.06 |
| ASTPwin | 16,023 | 1.13 | −0.10 | 0.995 | 1.00 | 0.97 | 0.03 | 0.13 | 0.13 | 9.7 | 1.04 | 0.12 |

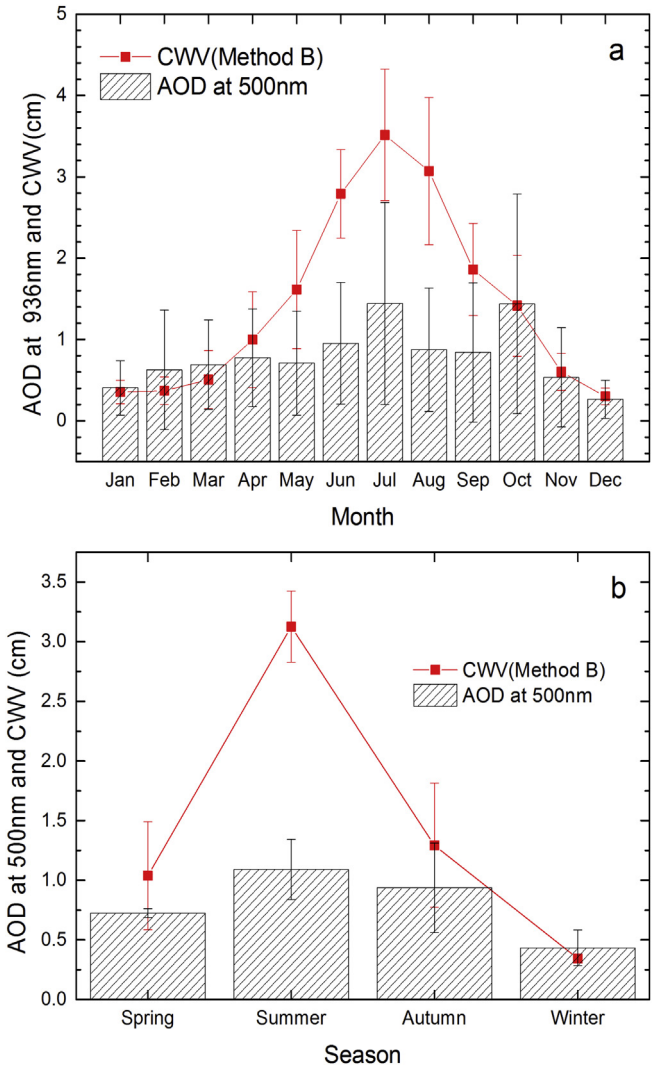


**Fig. 6.** The (a) monthly and (b) seasonal averaged values and standard deviations of CWV (Method B) and $AOD_{500nm}$.

vapor (Holben et al., 1998; Smirnov et al., 2004). According to the conditions of the data screening, five clear days of direct solar radiation observational data in 2015 were selected. For Eq. (6), using the least-squares fitting line acquired the intercept of $ln(V_0R^{-2})$.The larger fitting line deviation points were then removed, and the fitting was performed again until the fitting line linear correlation was greater than or equal to 0.99. The calibration result is shown in Fig. 3.

Fig. 3 shows that the data of the five clear days fit into a linear distribution, and the fitting linear correlation coefficient was greater than 0.99. The calibration value $V_0$ could then be acquired by the intercept $ln(V_0R^{-2})$.

### 3.5. Calibration result

The calibration results of five eligible clear days compared with the original calibration are shown in Table 1.

From Table 1, two sets of data calibration values were higher than the original calibration value; the remaining three calibration values were lower. The errors of the calibration values of all five clear days were within ±9%, and the calibration results were basically the same as the original calibration value. The mean value of the five sets of data was $V_0 = 16{,}990$, deviating from the average original values at about 4%, which is allowable according to the specification. From the calibration results it can be concluded that, for the calibration values of the 936 nm water vapor channel, the modified Langley method is feasible and preferential. However, the calibration value and original calibration value demonstrate a certain deviation. This is due to the long-term field observation of the sunphotometer, uncertainty in the natural environment, and instrument wear, amongst other factors. What's more, we should better control the objective conditions during the calibration process, but it's really hard to find the condition which $AOD_{500nm}$ is smaller than 0.05 in Beijing urban areas, so we will do the further research at high altitude sites in the future.

## 4. CWV retrieval results

Removing the highest and lowest value, we took the average calibration value of the remaining three clear days as the calibration value of the 936 nm water vapor channel. Using Methods A, B and C to retrieve the CWV of these five clear days for urban Beijing, comparisons were made with the CWV of the AERONET Beijing-CAMS site. The combined influence of systematic and random uncertainties can induce a total estimated uncertainty of CWV retrievals by AERONET approximately 12–15% (Pérez-Ramírez et al., 2014). Table 2 and Fig. 4 show the CWV retrieved using the different methods and the correlation coefficients and comparison results.

Under the condition of a relatively stable atmosphere, the optical thickness changed little, when comparing Methods A, B and C to AERONET. The results showed high correlation for Methods A, B and C with AERONET; the correlation coefficients were all above 0.90. This indicates that Methods A, B and C are highly feasible for retrieving CWV. Comparing the correlation coefficients of Methods A, B and C with AERONET, Method B (AERONET algorithm) and AERONET have the nearest value (correlation coefficient of 0.993), but their results are slightly different, possibly due to the calibration error and algorithm accuracy. The correlation coefficient of Method C and AERONET was 0.991, and Method C was nearer to AERONET compared with Method A. This indicates that Method C is more reasonable, and Method A produces larger error.

Fig. 5a–c show the fitting of AERONET with Method B, Method C and ASTPWin, respectively. The statistical results are summarized in Table 3. Fig. 5d–f show intercomparison fittings of Method B, Method C and ASTPWin. As can be seen, AERONET and Method B, Method C and ASTPWin were highly correlated, indicating that these three methods can be used to acquire CWV. The differences between each method and AERONET product range from 5.9% to 9.7% (rms). The mean difference are within ±0.08 cm, and the mean ratios range from 0.92 to 1.04. Comparing the fitting results, the three methods shows light differences. The fitting coefficient of Method C and AERONET was larger than that for ASTPWin and AERONET. The fitting coefficient of Method C and ASTPWin was 0.988, and the slope was 0.952, demonstrating that the CWV retrieval result of Method C was in line with the ASTPWin results. Meanwhile, the fitting coefficient of Method C and AERONET was 0.995, and the slope was 1.087, showing that the CWV retrieval results of Method C and AERONET were highly correlated. This indicates that, as long as the calibration value is accurate, Method C is an accurate CWV retrieval method. The CWV value of Method C was smaller than that of Method B, possibly due to neglecting $m(\tau_1-\tau_2)$.However, the causes require further study.

Fig. 6a and b show the monthly and seasonal averaged values and standard deviations of CWV (Method B) and $AOD_{500nm}$, respectively. Fig. 6a indicates that the variation trends of the monthly averaged values of CWV and $AOD_{500nm}$ were similar, with the maximum occurring in July and the minimum in December.

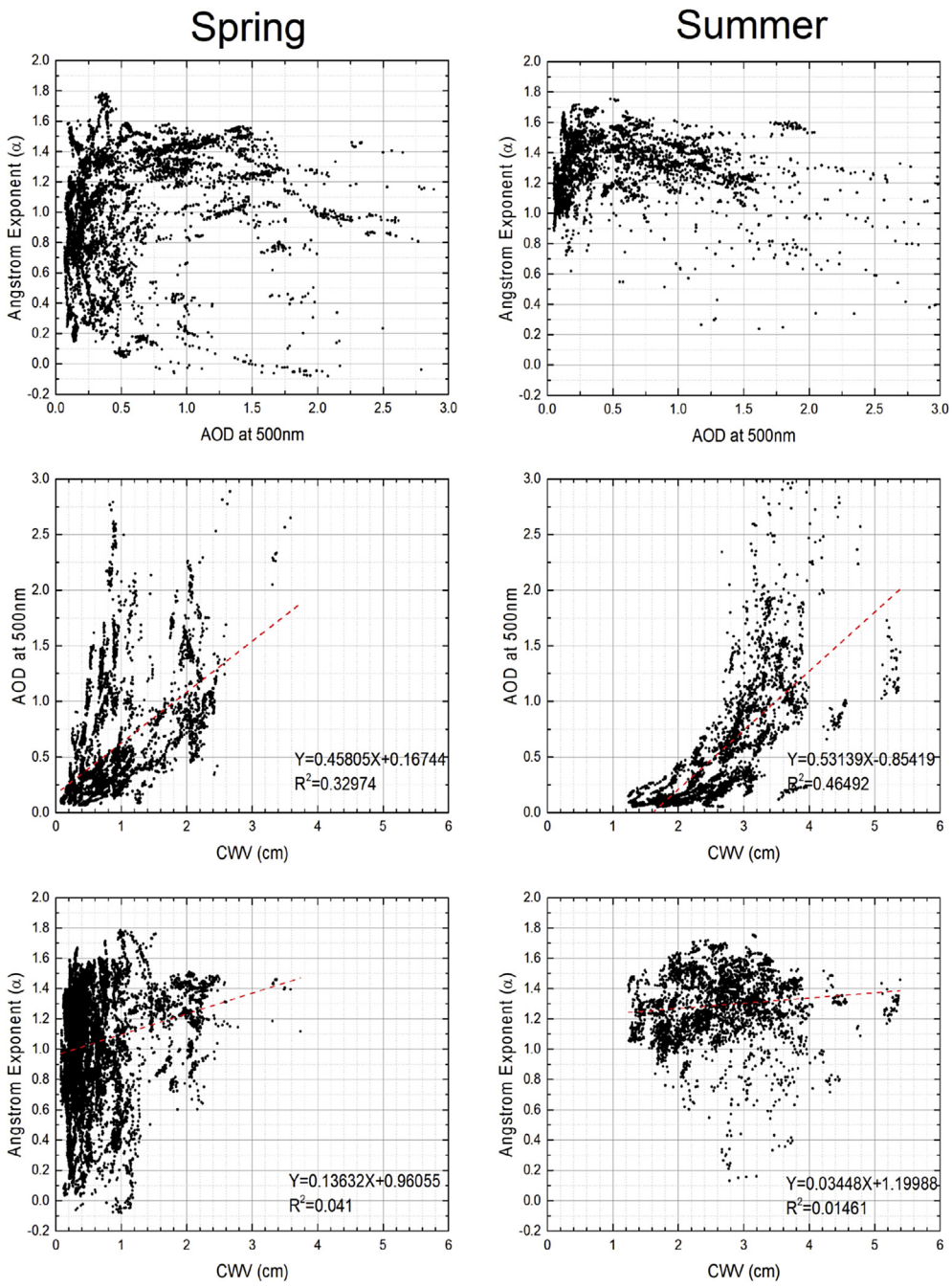


**Fig. 7.** Seasonal scatter graphs of the Ångström parameter vs. the AOD, the AOD vs. the CWV, and the Ångström parameter vs. the CWV.

Because of the high incidence of haze in October, the $AOD_{500nm}$ was higher than usual. Fig. 6b indicates that the variation trends of seasonal averaged values of CWV and $AOD_{500nm}$ were similar, but in the following order: summer > autumn > spring > winter.

The seasonal scatter graph of the AOD versus the Ångström parameter ($\alpha_{440-870}$) is shown in Fig. 7. Two different distribution types can be seen in spring. One is an increasing AOD with a decreasing Ångström exponent, representing coarse particles. And the other is an increasing AOD with an increasing $\alpha$, representing fine particles. The summer is mainly characterized by fine particles. Spring, autumn and winter are a mix of coarse and fine particles. The seasonal relationship between CWV and AOD at 500 nm shows a notable correlation; the four seasons feature increasing AOD with increasing CWV, reflecting the hygroscopicity of aerosol fine particle growth characteristics. This feature is more obvious in summer and winter; in summer, the correlation coefficient is approximately 0.68, and for the whole dataset their correlation can be calculated as follows:

$$AOD_{500nm} = 0.53 \times CWV + 0.85.$$

In winter, the correlation coefficient is about 0.65, and for the whole dataset their correlation can be calculated as follows:

$$AOD_{500nm} = 1.56 \times CWV + 0.20.$$

For the seasonal relationship between CWV and $\alpha$, there are no obvious characteristics, and this may be related to the aerosol chemical composition.

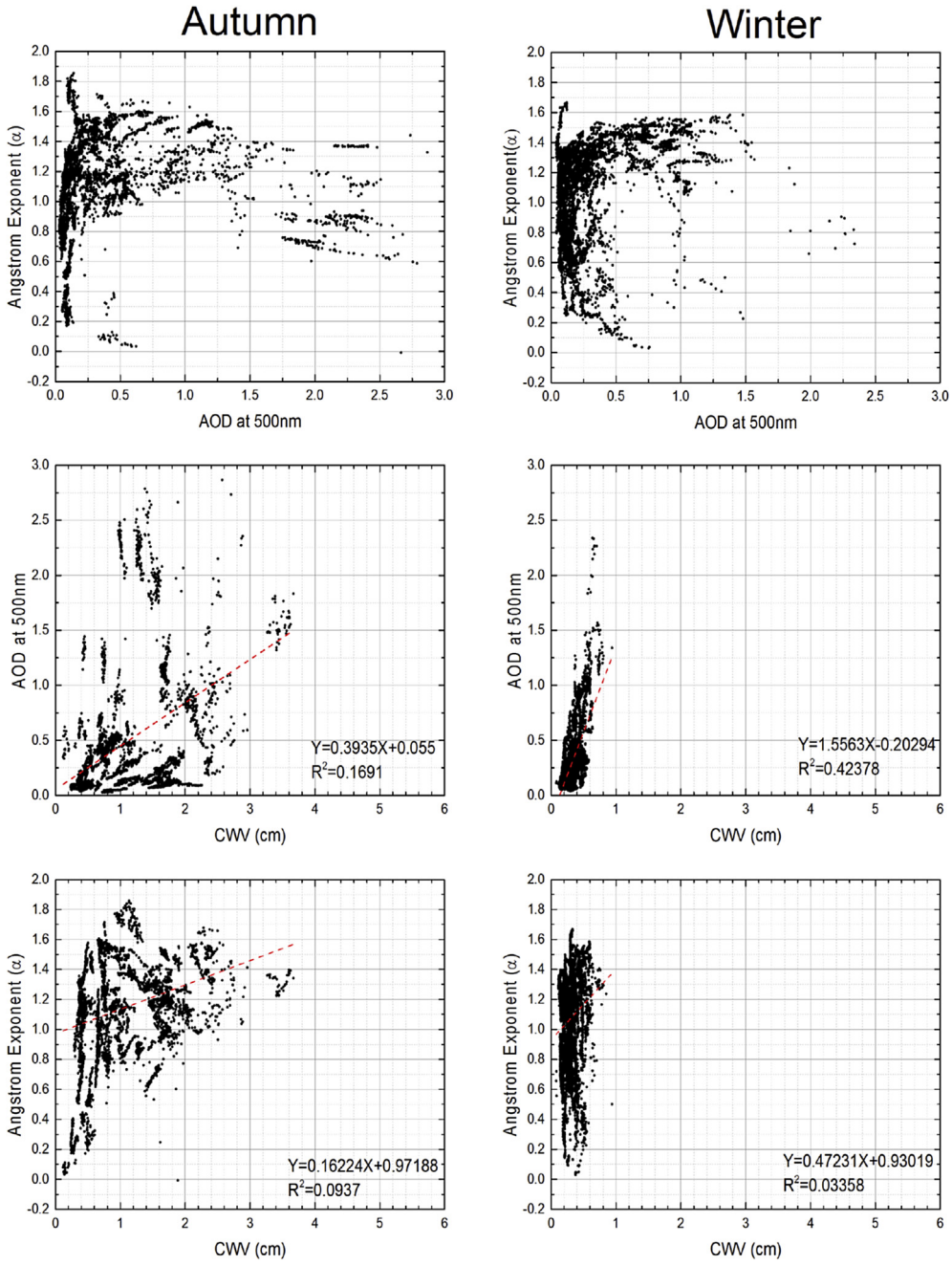


**Fig. 7.** *continued*

## 5. Conclusion

This paper presents a process for the calibration of the 936 nm water vapor channel, and the CWV retrieval results over urban Beijing. The main conclusions of the study can be summarized as follows:

1. The modified Langley method can be used to calibrate the 936 nm water vapor channel of the CE318 sunphotometer. The calibration value deviates from the original values, but only by about 4%; the average deviation is within the range of allowable error. The parameter sensitivity test showed that different values of pressure, altitude and $AOD_{936nm}$ have a great influence on the calibration value. Therefore, in order to acquire an accurate calibration value, these sensitivity parameters should be considered. Meanwhile, data screening and accurate fitting values of the constants *a* and *b* are still especially important. For the sake of an accurate calibration value and error reduction, a suitable wild field for the calibration should be chosen.
2. The CWV retrieval results showed that ASTPWin, Method B and Method C were highly correlated with AERONET. All three methods, therefore, can be used to retrieve the CWV. The fitting coefficient of Method C and AERONET was 0.995, and the slope was 1.087, demonstrating that the CWV retrieval results of Method C and AERONET were highly correlated. This suggests that, as long as the calibration value is accurate, Method C is a relatively accurate CWV retrieval method. This also implies that the modified Langley method is feasible and preferential with respect to the calibration of the 936 nm water vapor channel.

3. The variation trends of the monthly averaged values of CWV and $AOD_{500nm}$ were similar, with the maximum occurring in July and the minimum in December. The variation trends of the seasonal averaged values of CWV and $AOD_{500nm}$ were similar, but could be placed in the following order: summer > autumn > spring > winter. The seasonal variation of $\alpha_{440-870}$ versus $AOD_{500nm}$, $\alpha_{440-870}$ versus CWV, and $AOD_{500nm}$ versus CWV, showed an increasing $AOD_{500nm}$ with increasing CWV. Summer was mainly characterized by fine particles; while spring, autumn and winter were a mix of coarse and fine particles, showing typical urban aerosol properties.

The work presented in this paper establishes a number of CWV retrieval methods for CARSNET. However, all of the data and CWV retrieval methods used in this study are based on ground-based remote sensing. To increase the accuracy of CWV retrieval, future work will incorporate global positioning system, microwave radiometer, and other technologies.

## Conflict of interest

There is no conflict of interest.

## Acknowledgments

This research was funded by the National Key Project of Basic Research (2011CB403401), the Project (41275167 & 41590874) supported by the National Natural Science Foundation of China, Strategic Priority Research Program of the Chinese Academy of Sciences (XDA05100301), CAMS Basis Research Project (2014R17) and the Climate Change Special Fund of CMA (CCSF201504). The research leading to these results has received funding from the European Union Seventh Framework Programme (FP7/2007-2013) under grant agreement no 262254.

## References

Alexandrov, M.D., Schmid, B., Turner, D.D., Cairns, B., Oinas, V., Lacis, A.A., Gutman, S.I., Westwater, E.R., Smirnov, A., Eilers, J., 2009. Columnar water vapour retrievals from multifilter rotating shadowband radiometer data. J. Geophys. Res. 114, D02306. http://dx.doi.org/10.1029/2008JD010543.

Angstrom, A., 1929. On the atmospheric transmission of sun radiation and on dust in the air. Geogr. Ann. 11, 156–166.

Bokoye, A.I., Royer, A., Cliche, P., O'Neill, N., 2007. Calibration of sun radiometer-based atmospheric water vapour retrievals using GPS meteorology. J. Atmos. Ocean. Technol. 24, 964–979. http://dx.doi.org/10.1175/JTECH2011.1.

Bruegge, C.J., Conel, J.E., Green, R.O., Margolis, J.S., Holm, R.G., Toon, G., 1992. Water vaporcolumn abundance retrievals during FIFE. J. Geophys. Res. 97, 18759–18768.

Campanelli, M., Lupi, A., Nakajima, T., Malvestuto, V., Tomasi, C., Estellés, V., 2010. Summertime columnar content of atmospheric water vapor from ground-based sun-sky radiometer measurements through a new in situ procedure. J. Geophys. Res. 115 http://dx.doi.org/10.1029/2009JD013211.

Campanelli, M., Nakajima, T., Khatri, P., Takamura, T., Uchiyama, A., Estellés Leal, V., Liberti, G.L., Malvestuto, V., 2014. Retrieval of characteristic parameters for water vapour transmittance in the development of ground based sun-sky radiometric measurements of columnar water vapour. Atmos. Meas. Tech. 7, 1075–1087.

Campmany, E., Bech, J., Rodríguez-Marcos, J., Sola, Y., Lorente, J., 2010. A comparison of total precipitable water measurements from radiosonde and sunphotometers. Atmos. Res. 97, 385–392.

Che, H., Zhang, X., Chen, H., Damiri, B., Goloub, P., Li, Z., Zhang, X., Wei, Y., Zhou, H., Dong, F., 2009. Instrument calibration and aerosol optical depth(AOD) validation of the China Aerosol Remote Sensing Network. J. Geophys. Res. 114, D03206.

Cimel, 2001. Sunphotometer User Manual Cimel CE-318, V.4.6. Cimel, 172 rue de Charonne, 75011 Paris, France, p. 79.

Galkin, V.D., Leiterer, U., Alekseeva, G.A., Novikov, V.V., Pakhomov, V.P., 2010. Accuracy of the Water Vapour Content Measurements in the Atmosphere Using Optical Methods eprint arXiv:1010.3669.available (free access without time limit) at: http://arxiv.org/abs/1010.3669 (accessed 7 April 2011, 2010).

Goloub, P., Li, Z., Dubovik, O., Blarel, L., Podvin, T., Jankowiak, I., Lecoq, R., Deroo, C., Chatenet, B., Morel, J.P., Cuevas, E., Ramos, R., 2007. PHOTONS/AERONET sunphotometer network overview: description, activities, results. P. SPIE 2007 (6936), 69360V. http://dx.doi.org/10.1117/12.783171.

Halthore, R.N., Markha, B.L., Deering, D.W., 1992. Atmospheric correction and calibration during Kurex-91, IGARSS'92. Int. Geosci. Remote Sens. Symp. 2, 1278–1290.

Halthore, R.N., Eck, T.F., Holben, B.N., Markham, B.L., 1997. Sun photometric measurements of atmospheric water vapor column abundance in the 940-nm band. J. Geophys. Res. 102, 4343–4352.

Hansen, J.E., Travis, L.D., 1974. Light scattering in planetary atmospheres. Space. Sci. Rev. 16, 527–610.

Holben, B.N., Eck, T.F., Slutsker, I., Tanre, D., Buis, J.P., Setzer, A., Vermote, E., Reagan, J.A., Kaufman, Y.J., Nakajima, T., 1998. AERONET—A federated instrument network and data archive for aerosol characterization. Remote. Sens. Environ. 66, 1–16.

Ingold, T., Schmid, B., Mätzler, C., Demoulin, P., Kämpfer, N., 2000. Modeled and empirical approaches for retrieving columnar water vapor from solar transmittance measurements in the 0.72, 0.82, and 0.94 μm absorption bands. J. Geophys. Res. 105, 24327–24343.

Josefsson, W., 1986. Solar Ultraviolet Radiation in Sweden. SMHI Rapporter Meteorologi Och Klimatologi (Sweden).

Kasten, F., Young, A.T., 1989. Revised optical air mass tables and approximation formula. Appl. Opt. 28, 4735–4738.

Kneizys, F.X., Shettle, E.P., Abreu, L.W., Chetwynd, J.H., Anderson, G.P., 1988. User's Guide ToLOWTRAN -7. Air Force Geophysics Laboratory Tech. Rep[R]. AFGL-TR-88–0177.

Livingston, J., Schmid, B., Redemann, J., Russell, P.B., Ramirez, S.A., Eilers, J., Gore, W., Howard, S., Pommier, J., Fetzer, E.J., Seemann, S.W., Borbas, E., Wolfe, D.E., Thompson, A.M., 2007. Comparison of water vapor measurements by airborne sun photometer and near-coincident in situ and satellite sensors during INTEX/ITCT 2004. J. Geophys. Res. 112 (D12).

Michalsky, J.J., Liljegren, J.C., Harrison, L.C., 1995. A comparison of sunphotometer derivations of total column water vapor and ozone to standard measures of same at the Southern Great Plains atmospheric radiation measurement site. J. Geophys. Res. 100, 25,995–26,003.

Pérez-Ramírez, D., Whiteman, D.N., Smirnov, A., Lyamani, H., Holben, B.N., Pinker, R., Andrade, M., Alados-Arboledas, L., 2014. Evaluation of AERONET precipitable water vapor versus microwave radiometry, GPS, and radiosondes at ARM sites. J. Geophys. Res. 119 (15), 9596–9613.

Plana-Fattori, A., Legrand, M., Tanré, D., Devaux, C., Vermeulen, A., Dubuisson, P., 1998. Estimating the atmospheric water vapor content from sun photometer measurements. J. Appl. Meteorol. 37, 790–804.

Reagan, J.A., Thome, K.J., Herman, B.M., 1992. A simple instrument and technique for measuring columnar water vapor via near-IR differential solar transmission measurements. IEEE Trans. Geosci. Remote. Sens. 30, 825–831.

Rothman, L.S., Barbe, A., Benner, D.C., Brown, L.R., Camy-Peyret, C., Carleer, M.R., Chance, K., Clerbaux, C., Dana, V., Devi, V.M., Fayt, A., Flaud, J.M., Gamache, R.R., Goldman, A., Jacquemart, D., Jucks, K.W., Lafferty, W.J., Mandin, J.Y., Massie, S.T., Nemtchinov, V., Newnham, D.A., Perrin, A., Rinsland, C.P., Schroeder, J., Smith, K.M., Smith, M.A.H., Tang, K., Toth, R.A., Vander Auwera, J., Varanasi, P., Yoshino, K., 2003. The HITRAN molecular spectroscopic database: edition of 2000 including updates through 2001. J. Quant. Spectrosc. Radiat. Transf. 82 (1), 5–44.

Rothman, L.S., Jacquemart, D., Barbe, A., Benner, D.C., Birk, M., Brown, L.R., Carleer, M.R., Chackerian Jr., C., Chance, K., Coudert, L.H., Dana, V., Devi, V.M., Flaud, J.M., Gamache, R.R., Goldman, A., Hartmann, J.M., Jucks, K.W., Maki, A.G., Mandin, J.Y., Massie, S.T., Orphal, J., Perrin, A., Rinsland, C.P., Smith, M.A.H., Tennyson, J., Tolchenov, R.N., Toth, R.A., Vander Auwera, J., Varanasi, P., Wagner, G., 2005. The HITRAN 2004 molecular spectroscopic database. J. Quant. Spectrosc. Radiat. Transf. 96, 139–204. http://dx.doi.org/10.1016/j.jqsrt.2004.10.008.

Schermaul, R., Learner, R.C.M., Newnham, D.A., Williams, R.G., Ballard, J., Zobov, N.F., Belmiloud, D., Tennyson, J., 2001a. The water vapor spectrum in the region 8600–15000 $cm^{-1}$: experimental and theoretical studies for a new spectral line database. I—Laboratory measurements. J. Mol. Spectrosc. 208, 32–42.

Schermaul, R., Learner, R.C.M., Newnham, D.A., Ballard, J., Zobov, N.F., Belmiloud, D., Tennyson, J., 2001b. The water vapor spectrum in the region 8600–15000 $cm^{-1}$: experimental and theoretica lstudies for a new spectral line database. II—Linelist construction. J. Mol. Spectrosc. 208, 43–45.

Schmid, B., Michalsky, J.J., Slater, D.W., Barnard, J.C., Halthore, R.N., Liljegren, J.C., Holben, B.N., Eck, T.F., Livingston, J.M., Russell, P.B., 2001. Comparison of columnar water-vapormeasurements from solar transmittance methods. Appl. Opt. 40, 1886–1896.

Schmid, B., Thorne, K., Demoulin, P., Peter, R., Mätzler, C., Sekler, J., 1996. Comparison of modeledand empirical approaches for retrieving columnar watervapor from solar transmittance measurements in the 0.94-μm region. J. Geophys. Res. 101, 9345–9358.

Smirnov, A., Holben, B.N., Eck, T.F., Dubovik, O., Slutsker, I., 2000. Cloud-screening and quality control algorithms for the AERONET database. Remote. Sens. Environ. 73, 337–349.

Smirnov, A., Holben, B.N., Lyapustin, A., Slutsker, I., Eck, T.F., 2004. AERONET Processing Algorithms Refinement: Proceedings of AERONET Workshop, El Arenosillo. NASA/GSFC Aeronet Project, Spain.

Tao, R., Che, H., Chen, Q., Wang, Y., Sun, J., Zhang, X., Lu, S., Guo, J., Wang, H., Zhang, X., 2014. Development of an integrating sphere calibration method for Cimel sunphotometers in China aerosol remote sensing network. Particuology 13, 88–99.

World Meteorological Organization Global (WMO), 2005. World Meteorological Organization Global Atmosphere Watch Experts Workshop on a Global Surface-based Network for Longterm Observations of Column Aerosol Optical Properties. GAW Technical Report. 162, TD 1287, Davos, 8–10 March 2004.

Zhang, H., Zheng, Y., Cai, Z., Pan, Z., 2009. Retrieval of atmospheric column water vapor content over zhengzhou with sunphotometer. Meteor. Sci. Technol. 37, 576–578.

Zhang, Y., Li, X., Gu, X., 2006. Estimation of water vapor amount over Beijing from sun photometer measurements. J. Remote. Sens. 10, 749–755 (in Chinese).

Zhou, N., Liu, M., 2011. Total column water vapor retrieval methods and results comparison by using sun photometer. Yaogan Xuebao-J. Remote. Sens. 15, 568–572 (in Chinese).